Chapter 2
Organic Semiconductor Growth and Transistor Performance as a Function of the Density of the Octadecylsilane Dielectric Modification Layer

2.1 Introduction

The central research focus in organic electronics has been improvement of charge transport in organic thin film transistors (OTFTs), the building blocks of organic circuits [1, 2]. Charge transport takes place primarily within the first few monolayers of semiconductor at the dielectric/semiconductor interface; therefore device performance is dominated by the properties of these interfacial layers [3, 4]. As aforementioned, grain boundaries between crystalline domains affect device performance, acting as barriers to charge transport [1, 5, 6]. Consequently, highly crystalline films deposited via a layer-by-layer 2D growth mode are desirable due to less energetically severe in-plane boundaries.

Octadecylsilanes (OTS), specifically octadecyltrimethoxysilane (OTMS) and octadecyltrichlorosilane (OTCS), have been widely used to modify the SiO_2 dielectric surface and have resulted in dramatic improvement of the field-effect mobility for a variety of semiconductors [4, 7–10]. In fact OTS modified SiO_2 is the most common surface for analyzing organic semiconductors [1, 2]. The hydrophobic nature of OTS is thought to passivate the SiO_2 surface, increase semiconductor crystal quality, reduce interfacial trap states and in some cases planarize the surface [5, 11, 12]. Previous reports have attributed the improvement of mobility on OTS-treated surfaces to a drastic reduction in surface energy by hydrophobic surface modification [13, 14]. However, a wide range of charge-carrier mobilities have been reported by a number of research groups for the same organic semiconductor on OTS, suggesting the need to understand the nature of the underlying OTS layer. For example, the reported mobilities of pentacene, the most widely studied semiconductor, OTFTs with OTS-modified SiO_2 ranges from 0.03 to greater than 2.0 $cm^2\ V^{-1}\ s^{-1}$ [1, 15]. This reflects the difference in a technologically useless semiconducting thin film (0.03 $cm^2\ V^{-1}\ s^{-1}$) to semiconducting thin film whose mobility (2.0 $cm^2\ V^{-1}\ s^{-1}$) exceeds that of amorphous silicon.

A. Virkar, *Investigating the Nucleation, Growth, and Energy Levels of Organic Semiconductors for High Performance Plastic Electronics*, Springer Theses,
DOI: 10.1007/978-1-4419-9704-3_2, © Springer Science+Business Media, LLC 2012

Previous work has shown that both inorganic and organic materials growth is highly sensitive to the chemical nature, packing, and defects of the underlying self-assembled monolayer (SAM) [16]. Recently, Cho and co-workers studied the dependence of pentacene TFTs on OTS order. They found improved pentacene TFT performance when the OTS layer was prepared at lower temperatures so that the monolayer was ordered [17]. However, conclusive and quantitative reasons for the differences in growth mode, and number of transistors tested were not discussed. In fact, prior to the research presented in this thesis, there has been almost no quantitative experimental research into nucleation and thin film growth of pentacene on organic surfaces (like OTS) even though they are more useful and common than inorganic ones like bare (unmodified) SiO_2. This is primarily because forming a reproducible OTS layer has been challenging. Cho and co-workers suggested that a lower nucleation density is observed on ordered OTS due to a greater pentacene diffusivity (see Chap. 3). In an earlier report, Cho and co-workers studied the chain length dependence of alkyl-silane treated SiO_2 on pentacene TFTs. In that report they found that pentacene diffusivity was the largest and nucleation density was the lowest on the most disordered shorter chained alkylsilanes [17]. However, in both of these reports the role of the surface on heterogeneous nucleation was not considered, which is the focus of the next two chapters, and is a major factor governing OTFT performance. The incongruence in Cho and co-workers' results stems from the fact that both growth mode and nucleation density are highly sensitive to the surface. Furthermore, models which have been developed for inorganic nucleation and thin film growth often fail to accurately represent organic thin film growth due to the differences in molecular symmetry and bonding.

In addition, some semiconductors only show marginally improved performance on any OTS treated surface compared to SiO_2 despite the large difference in surface energy [5]. This suggests, as Markov and others have theorized, that each combination of molecule and substrate must be considered unique [18, 19]. The most relevant factor affecting growth, and consequently charge carrier mobility, is the specific energetic interaction between the semiconductor and the surface [18, 19]. This interaction is influenced considerably by the phase of the underlying OTS monolayer, even though all the OTS phases studied have identical chemical compositions and similar surface energies and roughness.

2.2 Fabrication and Characterization of Octadecylsilane Monolayers

In the study presented in this chapter, the effect of density and degree of ordering of OTS monolayers on the performance of two of the most widely studied and highest mobility thin film organic semiconductors: pentacene (p-channel) and C_{60} (n-channel) was investigated [1, 4, 5, 11, 20–24]. The Langmuir–Blodgett (LB)

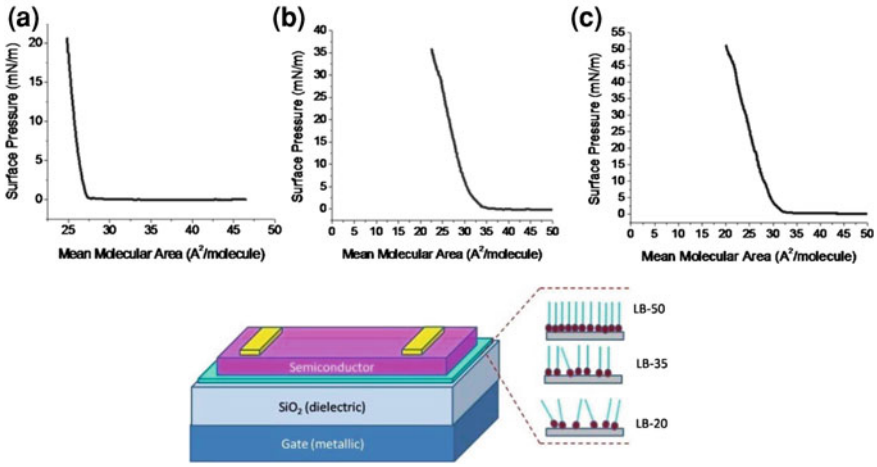

Fig. 2.1 Representative surface pressure-area isotherms for **a** LB-20 mN m^{-1}. (LB-20), **b** LB-35 mN m^{-1} (LB-35), and **c** LB-50 mN m^{-1} (LB-50). The typical film collapse pressure was 55 mN m^{-1}. Below is a schematic highlighting that the only variable between the transistors studied was the underlying order of the OTS SAM

technique was employed to systematically vary the organization and density of the OTS monolayers. In this well-known ultrathin-film deposition technique, amphiphilic OTS molecules are compressed by applying a lateral pressure to the monolayer film at the air–water interface [25]. Under increasing applied lateral pressure, the film undergoes a transition from a 2D gas to a 2D liquid and finally to an ordered 2D solid [25]. From the Langmuir isotherms obtained in our study, the OTS film collapses at a surface pressure of $\sim$55 mN m^{-1} and there appears to be a phase transition leading to the most ordered phase at a surface pressure of $\sim$40mN m^{-1} (Fig. 2.1). This phase change from one condensed (2D solid) phase to another condensed phase was also observed by Duran and co-workers [26]. Accordingly, surface pressures of 20, 35, and 50 mN m^{-1} were chosen to study OTS films of different degrees of order (designated as LB-20, LB-35 and LB-50). Moreover, by studying LB-35 and LB-50 we were able to probe two distinct condensed phases. During fabrication of the Langmuir films, OTMS molecules were hydrolyzed and partially polymerized on the trough at pH of 3 [26]. The polymerized monolayer was Blodgett-transferred to the thermally grown silicon oxide (300 nm) surface on a heavily doped silicon wafer, which is used as the gate electrode. For comparison, the commonly used OTMS-V and OTCS-V vapor deposited films were also prepared. These vapor deposited films are considerably less dense than the LB films, and are more susceptible to inconsistencies in film properties since they cannot be fabricated in a controlled way like LB films [4, 27]. Transistors were completed in top contact geometry with gold source and drain electrodes (see Experimental). The channel length was 50 μm and the width was 1,000 μm. Thus the only variable probed was the order and density of the underlying OTS.

Table 2.1 Peak positions corresponding to the absorption maxima for the various CH_2 and CH_3 stretch modes probed using GATR-FTIR

Crystalline[a] (cm^{-1})	Liquid[a] (cm^{-1})	LB-50 (cm^{-1})	LB-35 (cm^{-1})	LB-20 (cm^{-1})	OTS-V (cm^{-1})
2,851	2,955	2,851	2,851	2,852	2,852
2,918	2,924	2,918	2,918	2,924	2,924
2,956	2,957	2,956	2,957	2,957	2,957

[a] Literature values for crystalline or liquid stretch modes from Ref. [28]

The OTS monolayers were characterized using grazing angle attenuated total reflectance Fourier transform infrared spectroscopy (GATR-FTIR) by examination of the C–H stretches of the CH_2 and CH_3 groups. Films transferred at higher surface pressures produced films with increased total absorption area, indicating an increased film density (Table 2.1 and Fig. 2.3a). This was accompanied by a characteristic shift of aliphatic vibrational stretching modes to lower wavenumbers (from 2,924 to 2,918 cm^{-1} for the asymmetric C–H stretch and from 2,855 to 2,851 cm^{-1} for the symmetric C–H stretch), indicating a transition from a liquid-like (disordered) to crystalline layer [28]. The magnitude of the observed peak shifts is similar to those reported in literature. The results are summarized in Table 2.1.

The OTS monolayers were further characterized using grazing incidence X-ray diffraction (GIXD). GIXD can probe in-plane order, and it is the ideal technique to study the crystalline order of a monolayer. Only the highly dense LB-50 monolayer gave rise to a Bragg rod in the GIXD spectrum (Figs. 2.2 and 2.6d). This indicates that indeed only the LB-50 monolayer has crystalline order. The calculated 4.2 Å hexagonal lattice constant for the LB-50 OTS is consistent with previous reports for crystalline OTS [29]. The LB-OTS peak does show some mild arching (Fig. 2.2). It is likely this tilt is due to the defects in the OTS film which arise from some ordered domains being non-coplanar with the majority of the film (Fig. 2.2c). Such defects can arise in LB films since the films are prepared by applying lateral compression.

The density and order of the LB films as a function of surface pressure were further characterized by ellipsometry, static water contact angle, and high resolution AFM (Table 2.2). As the monolayers were compressed, the film thickness and water contact angle increased, again indicating a denser monolayer. Using high resolution atomic force microcopy, it was determined that the LB films also showed larger overall domain size, roughly 30% larger than the vapor phase deposited films. The root mean square (RMS) roughness was similar for the LB films and the vapor deposited OTS-V film, confirming that lower mobilities observed for OTS-V treated OTFTs are not due to surface roughness effects [12, 13, 30]. The key film characteristics (C–H stretching mode frequencies, contact angle and surface roughness) for all the OTS films remained unchanged after heating to 200 °C under argon, indicating the films are stable and do not undergo thermal phase changes in the temperature ranges used for semiconductor deposition.

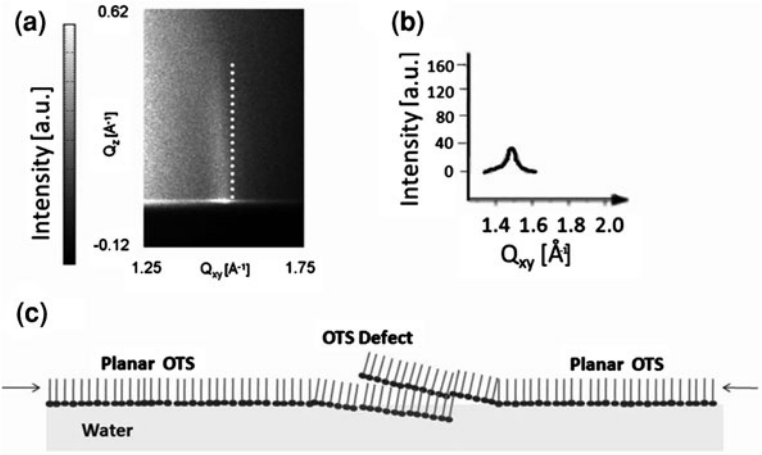

Fig. 2.2 **a** GIXD spectrum of LB-50 OTS monolayer. The white dotted line is drawn perpendicular to highlight the mild arching in the OTS peak. **b** Line profile of OTS LB-50 spectrum. **c** Schematic of OTS film on Langmuir trough showing potential defects which can arise during compression. The arrows indicate the direction of compression

Table 2.2 Properties of OTS monolayers studied

Sample	Mean molecular area (Å^2 molecular^{-1})	Height (nm)	Contact angle (deg)	RMS roughness (nm)
LB-20	24.8	2.0	101.7	0.2
LB-35	22.5	2.1	102.6	0.3
LB-50	20.1	2.1	104.1	0.2
OTS-V	28.7[a]	1.9	98.3	0.2

[a] The MMA values were estimated by calculating the area under absorption peaks from GATR-FTIR spectra for the OTS-V surface and comparing them to the area under the absorption peaks for the LB films with known MMA values

2.3 Effects of OTS Density on Pentacene and C60 Transistor Performance

The pentacene charge-carrier mobility (μ) extracted from saturation transfer characteristics is plotted as a function of the density [inverse mean molecular area (MMA)] of the OTS monolayer in Fig. 2.3c. The MMA is calculated based on the total number of molecules deposited on the Langmuir trough, and the total area occupied by the Langmuir film at the corresponding surface pressure. The average pentacene hole mobility measured for 50 devices on each type of OTS increases with increasing OTS density from 0.4 cm^2 V^{-1} s^{-1} for the least compressed LB film (LB-20) to 1.9 cm^2 V^{-1} s^{-1} on the most compressed (highest order) LB film (LB-50) despite only small differences in surface energy and roughness. This suggests that the density of OTS is a critical factor effecting performance. The mobility

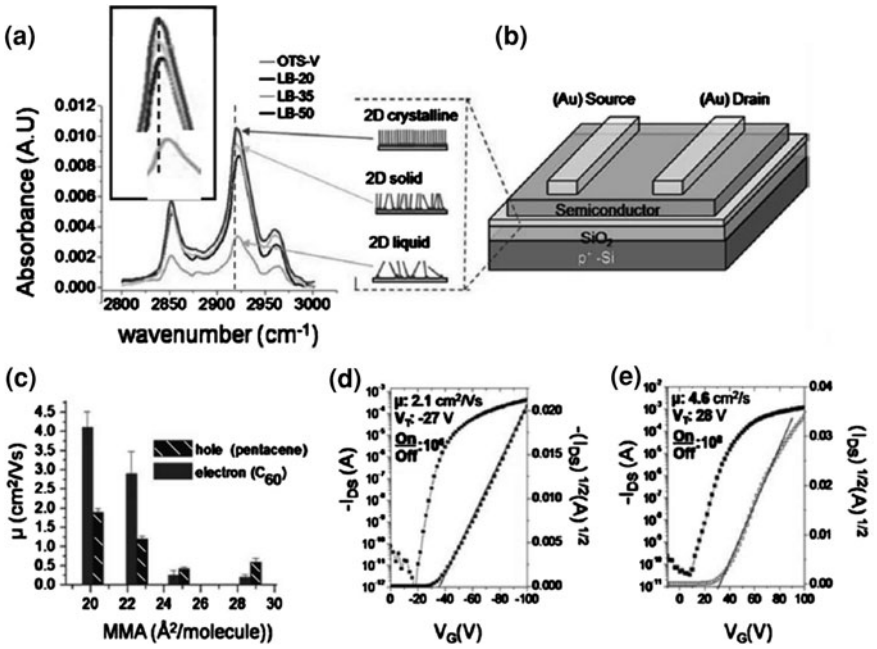

Fig. 2.3 **a**, **b** GATR–FTIR spectrum for the OTS films with differing 2D phases, and densities quantified by the mean molecular area MMA extracted from the Langmuir trough. **b** Schematic of pentacene OTFT with underlying OTS monolayers in different 2D phases. **c** The average (over 50 devices per OTS treatment) saturation mobility μ ($cm^2\ V^{-1}\ s^{-1}$) of 45 nm pentacene OTFTs measured in ambient and average (over 10 devices per OTS treatment) saturation mobility μ ($cm^2\ V^{-1}\ s^{-1}$) of 45 nm C_{60} OTFTs tested in a N_2 glovebox. The source–drain voltage was fixed at -100 V for p-channel transistors (pentacene), and 100 V for n-channel transistors (C_{60}). **d** Typical I–V transfer curves for pentacene TFTs with LB-50 OTS treatment. The mobility, threshold voltage and on/off ratios are provided as insets. **e** Typical I–V transfer curves for C_{60} TFTs with LB-50 OTS treatment. The mobility, threshold voltage VT and on/off ratios are provided as insets

on the less dense OTS-V (MMA = 28.7 $Å^2$ $molecule^{-1}$) is comparable to the lowest compressed LB film (20 m Nm^{-1}, MMA = 24.8 $Å^2$ $molecule^{-1}$) substrate despite lower film density. See Tables 2.3 and 2.4 for summary of average electrical characteristics. C_{60} OTFTs showed an electron mobility as high as 5.2 $cm^2\ V^{-1}s^{-1}$ (measured in a nitrogen glovebox) on the LB-50 film and followed the same trend as pentacene with mobility decreasing with decreasing OTS order. This C_{60} mobility on the dense OTS is amongst the highest reported in the literature [4, 24].

The pentacene TFTs were fabricated on four different days during four different depositions, and the C_{60} TFTs were deposited on two different days. For each respective set of devices the performance was very similar on LB-50 regardless of the deposition and the performance was consistently higher than the OTS-V treated TFTs. Both types of transistors showed negligible change in the threshold voltage on the various OTS surfaces, the on/off ratio was consistently above 10^5–10^6 and

the gate current was consistently several orders of magnitude lower than the drain current (see Figs. 2.4 and 2.5). For 50 μm channel length TFTs the contact resistances, are typically negligible compared to channel resistances; the device performance is dominated by the channel, and thus by the pentacene grains in the channel [31, 32]. From the output characteristics, the linear region of the IV curves show no non-linearity indicating the absence of contact issues. In order to test for the contribution of contact and channel resistances, several pentacene OTFTs with different channel lengths were tested and contact resistance was extracted. The contact resistances were nearly identical (within 3.0%) for TFTs fabricated on different OTS monolayers and were much smaller than the channel resistances indicating that indeed the channel effects dictate performance. (Fig. 2.5).

2.4 Organic Semiconductor Thin Film Analysis: Grazing Incidence X-ray Diffraction and Atomic Force Microscopy

In order to determine the effect of OTS monolayer density on organic semiconductor nucleation and growth at the semiconductor/dielectric interface, pentacene thin films (nominally 3 nm monitored by quartz microbalance during deposition) were deposited onto the OTS films under identical conditions as those used for OTFT fabrication. Due to the gate field, in the transistor's "on" state, the majority of charge carriers are induced and transported in the first $\sim$5 nm of semiconductor near the dielectric interface; the packing and morphology of the initially deposited interfacial layer is therefore critical [3, 33]. These were examined using atomic force microscopy (AFM) and grazing incidence X-ray diffraction (GIXD), giving information about the morphology and crystalline order of the pentacene monolayer film directly involved in charge transport. AFM was performed immediately after deposition to ensure that the film did not undergo reorganization. AFM was also performed before and after GIXD experiments to also ensure that films did not change during exposure to X-rays (typically for 30 min).

To determine if the packing of pentacene in the first monolayer is affected by the difference in OTS density, we carried out GIXD of the pentacene monolayers. The characteristic pentacene (11L), (02L) and (12L) in-plane Bragg rods are seen in the GIXD spectra (Fig. 2.6). On the LB-50 film (Fig. 2.6d), an additional broad peak between the (11L) and (02L) pentacene peaks is observed again due to the crystalline nature of the underlying OTS. The lattice constants of pentacene ($a = 5.93$ Å, $b = 7.58$ Å, $\gamma \approx 90°$) extracted from the diffraction peaks were nearly identical regardless of the OTS preparation method and are similar to those reported for pentacene grown on hexamethyldisilazane (HMDS) or OTS [34, 35]. The pentacene GIXD spectra (position of peaks in Q_{xy} and Q_z) are also similar on all the OTS surfaces. This indicates that the difference in mobility on different OTS surfaces is not due to different pentacene packing motifs. It is also interesting

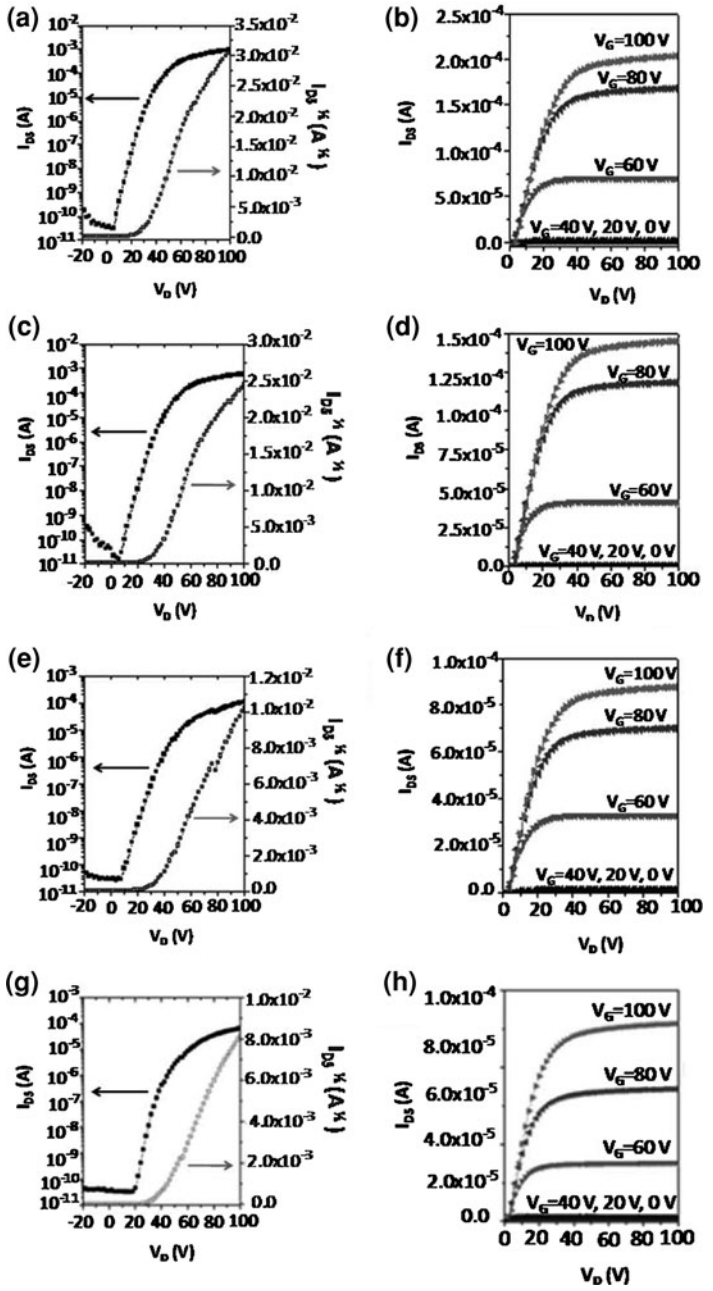

Fig. 2.4 Transfer and output curves for C_{60} 45 nm TFT on different OTS layer. **a** transfer curve LB-50, **b** output curves LB-50, **c** transfer curves LB-35, **d** output curves LB-35, **e** transfer curves LB-20, **f** output curves LB-20, **g** transfer curve OTS-V, **h** output curves OTS-V

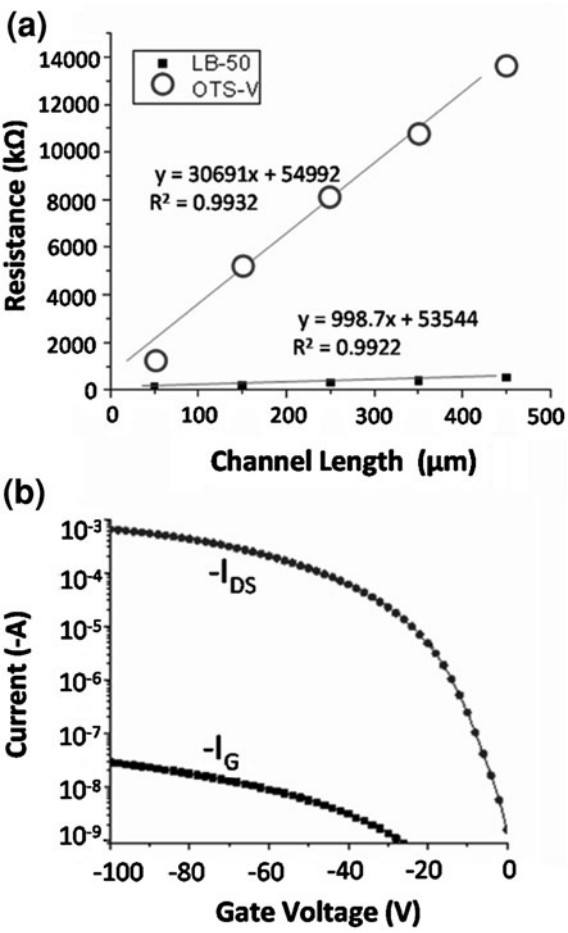

Fig. 2.5 **a** Resistance versus channel length for pentacene TFTs with OTS-V or LB-50 dielectric modification layers. The equation of the line of best fit and the corresponding R^2 value are provided on the graph. The equation is written in a $y = mx + b$ format, where m is the slope relating the resistance (y) to channel length (x), and extracting to $x = 0$ the contact resistance can be evaluated as b/2. Thus the extracted two point contact resistance for typical LB-50 TFTs is 2.67 kΩ and for OTS-V TFT is 2.75 kΩ. The difference in contact resistance is <3%. **b** Typical gate and drain currents for pentacene TFTs with LB-50 dielectric modification layers. Typical gate currents are orders of magnitude smaller than drain currents

to note there is an additional diffraction peak at $Q_{xy} = 1.6$ Å^{-1} on OTS-V (Fig. 2.6a) which corresponds to a portion of the film exhibiting the bulk pentacene phase. This 3D growth on OTS-V is further asserted by the AFM results discussed below. The full-width at half max (FWHM) of the diffraction peaks can be used to gauge the crystalline quality of the pentacene on various OTS surfaces. However, for all the films studied, the FWHM was resolution limited (domain size >10 nm) (see Experimental 2.7).

AFM of the nominally 3 nm pentacene films (Fig. 2.7) did, however, show a clear trend between thin film morphology and charge carrier mobility. The growth mode on the highly ordered LB films showed the more desirable 2D layer-by-layer (Frank-van der Merwe type) growth (Fig. 2.7d) as compared to the less favorable 3D (Volmer-Weber type) growth on OTS-V (Fig. 2.7a) which leads to many island severe grain boundaries after coalescence [1, 18, 19]. The growth mode on OTS-V is purely 3D island-type; no complete monolayer forms within the first 3 nm of

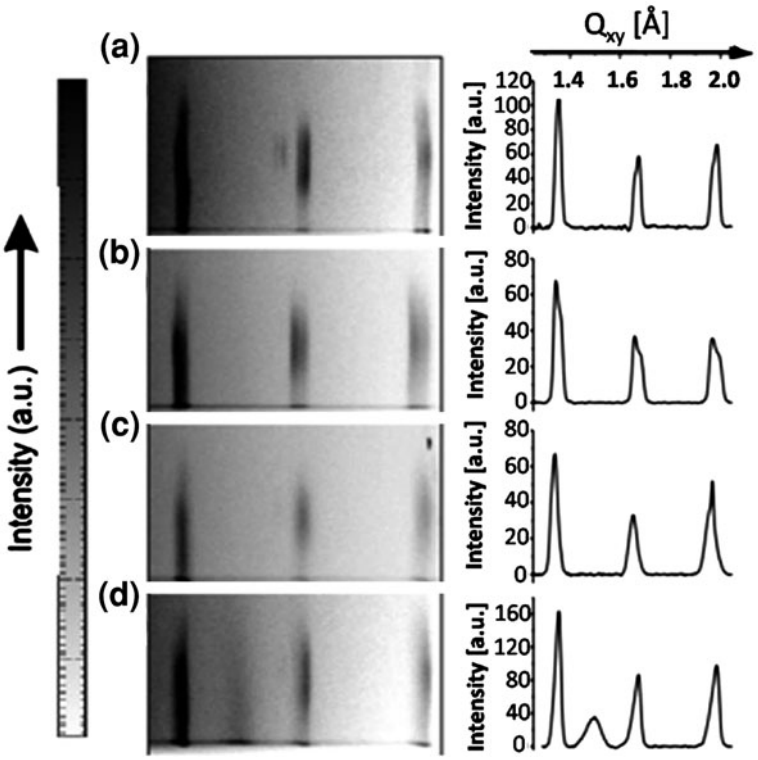

Fig. 2.6 Section of GIXD spectrum of 3 nm pentacene films deposited under identical conditions to those used in OTFT fabrication (0.3 Å s^{-1} at 60 °C) on: **a** OTS-V, **b** on LB-20 **c** LB-35, **d** LB-50 in all plots, Q_z (magnitude of scattering vector normal to the surface) is vertical. To the right of each GIXD spectrum are the corresponding line profiles which show the integrated peaks along Q_z. The corresponding values of Q_{xy} are also provided above the line profiles

nominal film thickness before additional layer growth, though the individual crystalline islands are large and terraced. The island size is considerably larger on OTC-V than on the LB films, which are composed of smaller connected islands. This is a critical observation: the growth mode has an enormous effect on the mobility even when the TFTs are fabricated using identical materials, at the same deposition conditions.

2.5 Organic Semiconductor Crystallization and 2D Versus 3D Growth Mode on OTS of Varying Order

Due to its paramount importance on the conductivity of thin films of pentacene, the 2D versus 3D growth mode for pentacene is described below and the strength of pentacene OTS interactions are estimated for the different surfaces. Moreover, the

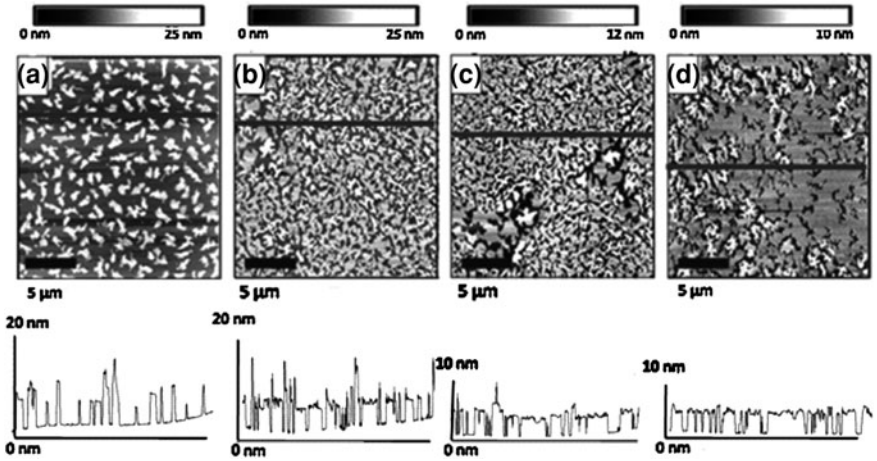

Fig. 2.7 Nominally 3 nm thin film of pentacene deposited under identical conditions as used in TFT fabrication (0.3 Å s^{-1} at 60 °C) on **a** OTS-V **b** OTS-20, **c** LB-35, **d** LB-50. The line corresponds to the profile shown directly below each AFM image. The growth mode of pentacene tends to be more and more 2D as the OTS density increases

interaction energies needed to drive 2D growth will be calculated, and related to the density of the underlying OTS.

It is important to note that the majority of this analysis considers a simple Kossel crystal (composed of cubes) since more complex crystals are often analytically impossible to analyze [18, 19]. The physics remain the same, but growth models are constructed from this simplified view so analytical expressions can be used and so that predictions of interaction energies are possible. For pentacene approximation as a Kossel crystal is reasonable since: (1) its molecular shape can be approximated as a rectangle, (2) the first monolayers of pentacene stand nearly upright on the substrate, i.e., $\sim$ zero tilt angle, (3) the molecules are symmetric (if you cut a standing pentacene molecule in the middle lengthwise, or in the center, the two halves are identical). (see Appendix for more the general thermodynamic derivation of the 2D versus 3D nucleation a Kossel crystal).

The formation of a 2D or 3D crystal is related to the chemical potential driving force for nucleation, the various surface energies of the crystal, the interfacial energies, and the molecule substrate interaction energy. The change in free energy for a finite sized pentacene crystal (which has two molecules in its unit cell) is related to the crystal size and the chemical potential by (Eq. 2.1, also see Fig. 2.8) [18, 19]:

$$\Delta G = -n_{ab}n_c 2\Delta\mu + [2n_b n_c \gamma_{100} + 2n_a n_c \gamma_{010} + 2n_d n_c \gamma_{1-10} + 2n_e n_c \gamma_{110} + n_{ab}(\gamma_{110} + \gamma_s)] \quad (2.1)$$

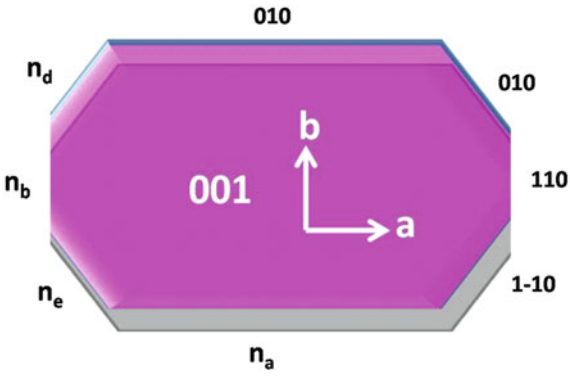

Fig. 2.8 The various facets of a large pentacene crystal. The number of unit cells corresponding to each surface is also given

where n_{ab} is the number of unit cells in the ab-plane, n_c is the number of unit cells in the c direction (how many unit cells high the crystal is), $\Delta\mu$ is the chemical potential difference between the vapor phase and the crystalline phase (of infinite size), n_a, n_b, n_d, and n_e, are the number of unit cells corresponding to the 010, 110, 110, and 1–10 surfaces. The specific surface energy terms (per unit cell) are denoted by γ_i (i again referring to the difference surfaces) and γ_s is the specific interfacial energy which relates the difference in interlayer interaction energy between layers of pentacene (γ_{001}) and between pentacene and the substrate ($\gamma_{mol-sub}$). More rigorously defined, it is the difference in energy (per unit cell) at the substrate, between interlayer adhesion energy and the adhesion energy of the surface (σ_i/A_{ab} where A_{ab} is the area per unit cell).

The critical cluster size, i.e., the number of unit cells needed to form a stable island, can be approximated by differentiation of (2.1) with respect to n_a, n_b, n_d, n_c, and n_e and equating to zero. Each solution is related to n_c* (the critical dimension of how many unit cells high the crystal is), $\Delta\mu$, and the surface/interaction energies. For discussion of 2D versus 3D growth mode n_c* is the most important term. The critical number of how many unit cells tall the crystal is, n_c, has the following solutions [19]:

$$n_c^* = \left\{ \left[\left(\frac{2(\gamma_{001} + \gamma_s)}{2\Delta\mu} \right), 1 \right] \right\}, \tag{2.2}$$

The first solution is for the 3D growth case (any size greater than 1 monolayer in height). The solution "1" of course is for the 2D crystal case. The solutions to the free energy at critical cluster size represent the energetic barrier which is needed to be overcome for nucleation. The solutions for a 3D and 2D crystal are given below [19]:

Table 2.3 Summary of pentacene TFT data measured in ambient conditions

Surface treatment	Average ($cm^2\ V^{-1}\ s^{-1}$)	Max ($cm^2\ V^{-1}\ s^{-1}$)	I_{on}/I_{off}	V_T (V)
LB-20	0.4 (0.05)	0.6	10^6	−18
LB-35	1.2 (0.08)	1.4	2×10^6	−24
LB-50	2.1 (0.12)	2.3	2×10^6	−20
OTS-V	0.6 (0.1)	0.9	10^6	−19

The values are average over ~50 devices for each OTS substrate treatment

Table 2.4 Summary of C_{60} OTFT data measured in a nitrogen glovebox

Surface treatment	Average ($cm^2\ V^{-1}\ s^{-1}$) (SD)	Max ($cm^2\ V^{-1}\ s^{-1}$)	I_{on}/I_{off}	V_T [V]
LB-20	0.3 (0.1)	0.4	3×10^5	35
LB-35	2.9 (0.5)	3.5	4×10^7	34
LB-50	4.1 (0.4)	5.3	3×10^7	33
OTS-V	0.2 (0.1)	0.3	2×10^6	40

The values are averaged over ten devices for each OTS substrate treatment

$$\Delta G^*_{3D} = \frac{4(\gamma_{001}+\gamma_s)[(2(\gamma_{010}+\gamma_{100})(\gamma_{110}+\gamma_{1-10})) - (2(\gamma^2_{010}+\gamma^2_{100})+\gamma^2_{110}+\gamma^2_{1-10})]}{(2\Delta\mu)^2} \tag{2.3}$$

$$\Delta G^*_{2D} = \frac{2[(\gamma_{010}+\gamma_{100})(\gamma_{110}+\gamma_{1-10})] - [2(\gamma^2_{010}+\gamma^2_{100})+\gamma^2_{110}+\gamma^2_{1-10}]}{2\Delta\mu - (\gamma_{001}+\gamma_s)} \tag{2.4}$$

Recall if ΔG^*_{3D} is lower, then 3D nucleation is favored, whereas if ΔG^*_{2D} is lower in energy than 2D nucleation is favored. From Eq. 2.3, 3D nucleation can occur for all supersaturations $\Delta\mu > 0$. For supersaturated systems, 2D nucleation can occur only once a supersaturation value $\Delta\mu_2$ has been achieved (see Appendix) [18],

$$\Delta\mu_2 = \frac{(\gamma_{001}+\gamma_s)}{2} = \gamma_{\text{interlayer}} - \gamma_{\text{mol-substrate}} \tag{2.5}$$

since at $\Delta\mu > \Delta\mu_2$ the solution to Eq. 2.5 becomes physically meaningful. As $\Delta\mu$ increases (beyond $\Delta\mu_2$), there is a transition where the barriers of nucleation for 2D and 3D nucleation become identical i.e. $(\Delta G^*_{2D} = \Delta G^*_{3D})$, and of course this means the 3D nuclei is one monolayer high or simply a 2D crystal! This value of critical supersatution ($\Delta\mu_{cr} = 2\Delta\mu_2$) is twice the transition where 2D nucleation becomes possible [18]. Of course for a given $\Delta\mu$, the differences in the interlayer and molecule–substrate interaction energies will dictate whether 2D or 3D nucleation is favored.

$$\Delta\mu_{cr} = 2\Delta\mu_2 = 2\left(\gamma_{\text{interlayer}} - \gamma_{\text{molecule-substrate}}\right) \tag{2.6}$$

So at $\Delta\mu \geq \Delta\mu_{cr}$, only 2D crystals are formed. The transition from 3D to 2D growth is one of the most important morphological criterions for high performance

pentacene transistors. Equation 2.6 is the most critical equation to analyze and investigate when considering the 2D vs 3D growth at the dielectric interface. For a fixed difference in chemical potential for pentacene deposited on the different surfaces, (i.e., same substrate temperatures and deposition rates) as is the case for the experiments presented in this chapter, Eq. 2.6 shows the growth mode is determined by the strength on the molecule–substrate interaction energy since the interlayer energy is a constant regardless of the underlying OTS. Recall that from the GIXD the lattice of pentacene is identical regardless of the OTS density.

In order to determine the strengths of interactions between pentacene and the various OTS monolayers with varying densities, the experimental conditions (deposition rate and substrate temperature) can be used to determine $\Delta\mu$ and thus by studying the nucleation and growth mode, the interaction energies can determined. It is also important to note that here it is assumed that the chemical potential difference is between the vapor phase of pentacene and an infinitely large crystal of pentacene (at the substrate temperature). The potential difference, $\Delta\mu$, can be expressed [18]:

$$\Delta\mu = \int_{P_c}^{P_v} \frac{\partial\mu_v}{\partial P} dP - \int_{P_c}^{P_v} \frac{\partial\mu_c}{\partial P} dP = \int_{P_c}^{P_v} (V_v - V_c) dP \tag{2.7}$$

where P is pressure, P_v is the vapor pressure during deposition and is related to the flux of molecules from the source, and P_c is equilibrium vapor pressure of the crystal at the substrate temperature. In Eq. 2.7 the second equality, the partial derivative of chemical potential in phase i with respect to pressure is equal to the molar volume (V) of phase i [19]:

$$\left(\frac{\partial\mu_i}{\partial P}\right)_{T,P} = V_i \tag{2.8}$$

which leads to the rightmost equality in Eq. 2.7. V_v is the molar volume of the vapor and V_c is the molar volume if the crystal. Since $V_v \ggg V_c$, and because the pressure used during vapor deposition is low enough to assume ideal gas behavior ($P \sim 10^{-6}$ torr) where $V_v = RT/P$, Eq. 2.7 can be rewritten:

$$\Delta\mu \approx RT \ln\left(\frac{P_v}{P_c}\right) \tag{2.9}$$

The equivalent vapor pressure (P_v) can be calculated as a function of the deposition rate (θ) and temperature using [36]:

$$\theta\left(\frac{\text{molecules}}{\text{cm}^2\,\text{s}}\right) = 3.51 \times 10^{22} \frac{P_v}{RT} \tag{2.10}$$

The equilibrium vapor pressure of a crystal (P_c) at substrate temperature T_{sub} is given by [19, 37]:

$$P_c = \exp\left(A - \frac{\Delta H_{\text{sub}}}{RT_{\text{sub}}}\right) \tag{2.11}$$

where ΔH_{sub} is the enthalpy of sublimation and A is a constant related to entropy and have been calculated elsewhere ($\Delta H_{\text{sub}} = 37.7$ kcal mol^{-1}) [37]. Combining Eqs. (2.9–2.11): the chemical potential driving force can be estimated from the heat of sublimation, and input experimental parameters:

$$\Delta\mu \approx \Delta H_{\text{sub}} + RT_{\text{sub}}[\ln((2\pi MRT_{\text{sub}})\theta) - A] \tag{2.12}$$

where R is the universal gas constant, T_{sub} is the substrate temperature, and M is the molecular weight of pentacene (278.4 g mol^{-1}) [18, 37]. For our pentacene deposition conditions (0.3 Å s^{-1} and a substrate temperature of 60 °C), $\Delta\mu$ is calculated from (2.12) to be 0.07 eV.

Finally, Eq. 2.6 can be analyzed and interaction energies for pentacene and the OTS with differing densities ($\gamma_{\text{mol-substrate}}$) can be approximated since now $\Delta\mu$ has been calculated, and $\gamma_{\text{interlayer}}$ is known. $\gamma_{\text{interlayer}}$ is approximately 0.13 eV, as has been well established from quantum simulations and experiments [19].

$$\Delta\mu_{cr} = 2\left(\gamma_{\text{interlayer}} - \gamma_{\text{molecule-substrate}}\right) \tag{2.6}$$

$\gamma_{\text{mol-substrate}}$ can then be estimated by determining the growth mode from AFM [19]. For OTS-V, $\gamma_{\text{mol-substrate}}$ is ca. $\sim$ 0.08–0.9 eV since the growth is highly 3D (also can be approximated by plugging into Eq. 2.4), while for the denser OTS films which engender 2D pentacene growth, $\gamma_{\text{mol-substrate}}$ is greater than 0.124 eV; this value is an important numerical heuristic to consider. For a crystalline layer of dense OTS like LB-50, the $\gamma_{\text{mol-substrate}}$ is actually greater than $\gamma_{\text{interlayer}}$ (as will be shown in detail in the next chapter). Nevertheless, what has been demonstrated is how strong the interaction energy between pentacene (deposited at typical conditions, i.e., rates and substrate temperatures) and the substrate must be in order for 2D growth to be possible. The numerical heuristic is important since one could imagine running simulations to determine the estimated pentacene surface interaction energy for a variety of surfaces to determine which ones give rise to suitable interaction energies needed to drive desirable 2D growth at the dielectric interface.

2.6 Conclusions

The most commonly used surface (an alkylsilane modified SiO_2) for organic transistors was investigated. The importance of phase and order of the organic dielectric surface modification layer for achieving 2D semiconductor film growth and high charge-carrier mobility in pentacene and C_{60}, two of highest performing organic semiconductors has been described. AFM and GIXD provide the first complete picture for the effect of both crystalline order and growth mode of the vital first few semiconductor monolayers on OTFT performance. These results

give insight into several new and important issues relevant to engineering high performance devices. Specifically, pentacene's (and many other semiconductors') thin-film growth is highly sensitive to the precise nature of the surface. An increase in density of the methyl terminated surface modification layer results in primarily two-dimensional growth of subsequently vacuum-deposited organic semiconductors. These changes in nucleation and growth give rise to a substantial improvement in the charge-transport characteristics in a number of materials, and suggest that this approach is generally important for the optimization of OTFT (as will be shown in Chap. 4). Finally, since the nucleation and growth mode were determined to be critical for OTFT performance, the chemical potential driving force for heterogenous pentacene crystallization was calculated. The interaction necessary to potentially engender 2D was also calculated. This knowledge may be invaluable and could lead researchers to use simulations to screen potential optimum dielectric materials. In the next chapter, the energetics of nucleation and stability of even thinner films of pentacene (prior to coalescence) are investigated in more detail on crystalline and amorphous OTS.

2.7 Experimental

2.7.1 Materials

Octadecyltrimethoxysilane (OTMS, 95%, purchased from Gelest Inc.) was purified by distillation and octadecyltrichlorosilane (OTCS, 99%, purchased from Gelest Inc.) was used as received. Device substrates consisted of heavily doped Si wafers with 300 nm of thermally grown silicon oxide having a capacitance per unit area (Ci) of 10 nF cm^{-2}. Pentacene was purchased from Sigma-Aldrich and sublimed twice prior to usage. C_{60} was purchased from Alfa Aesar (99.5%) and used as received. For ellipsometry and GIXD experiments, silicon wafers with 2–3 nm of native oxide were used. Prior to OTS treatment the wafers were cleaned with piranha (70:30 H_2SO_4:H_2O_2) for 60 min and then with ozone plasma (Jetlight UVO-cleaner Model 42–100 V) for 10 min.

2.7.2 Fabrication of OTS films

LB Films: A OTMS solution (1 mg ml^{-1} in chloroform) was prepared in a nitrogen glovebox and filtered (0.2 μm pore size). The trough (Nima model 612D) was filled with Millipore water (pH = 3) prepared using concentrated hydrochloric acid (38% HCl). The OTMS films were compressed (20 cm^2 min^{-1}) with respect to change in trough area to the desired surface pressure and then Blodgett-transferred (1 mm min^{-1}) to the Si/SiO_2 substrate. The substrates were cleaned

sequentially with toluene, isopropanol, acetone, distilled water and isopropanol again and then dried using a nitrogen gun (99.9% pure).

2.7.3 Characterization

The grazing angle attenuated total reflectance (GATR) spectrum was obtained using a Nicolet 6700 Fourier Transform Infrared Spectrometer (FTIR) using a germanium crystal.

A Sopra Bois–Columbes ellipsometer with a Physike Instrumente laser (He–Ne, $\lambda = 632.8$ nm, angle of incidence of 70°) and detector were used for OTS thickness measurements. Thickness was calculated from Ψ and Δ values and measured for five areas on the substrate. The following input refractive indices were used: air, $n_0 = 0$; alkylsilane, $n_1 = 1.450$; native silicon oxide, $n_2 = 1.460$, silicon, $n_3 = 3.873$, $k = -0.016$.

The AFM images of organic semiconductors were collected using a Digital Instruments MMAFM-2 scanning probe microscope. Tapping mode AFM was performed on the samples with a silicon tip with a frequency of 300 kHz.

2.7.4 High Resolution AFM

The OTS substrates were washed sequentially with ethanol (99.99% pure from Gold Shield Chemical Co.) and milli-Q water (18.3 MΩ) two times at room temperature (296 K) and allow to air dry before characterization using AFM. The OTS substrates were characterized in decahydronaphthalene solution (99.9%, Sigma-Aldrich).The optimum imaging area to visualize local domain is 100 × 100 nm under AFM. Thus, the cursor profile and RMS value was obtained using RHK-based imaging processing software at 100 × 100 nm area. For statistical analysis, both domain sizes (FWHM), separation (center-to-center and edge-to-edge) and vertical height were measured quantitatively from over ten cursor profiles per image, using characteristic features, at 300 x 300 nm areas. Repeat experiments yielded similar results.

2.7.5 Grazing Incidence X-ray Diffraction

GIXD was performed on the samples at the Stanford Synchrotron Radiation Lightsource (SSRL) on beam line 11–3 with a photon energy of 12.73 keV. A 2D image plate (MAR345) with effective pixel size of 150 μm (2,300 × 2,300 pixels) was used to detect the diffracted X-rays. The detector was 400.15 mm from the

sample center. The angle of incidence was fixed at 0.1°. The GIXD data was analyzed using FIT-2D and Peakfit software programs.

The resolution for GIXD was calculated using:

$$\Delta Q_{xy} = \frac{2\pi d \tan(2\theta)}{\lambda D} \tag{2.13}$$

where:
ΔQ_{xy} = in-plane resolution ($Å^{-1}$)
2θ = the scattering angle (degrees)
λ = X-ray wavelength (Å)
D = distance between the sample and the detector (cm)
d = sample length (cm)
Solving: $\Delta Q_{xy} = 0.06$ $Å^{-1}$

2.7.6 Electrical Characterization

A Keithley 2,400 semiconductor parameter analyzer was used to test p-channel transistors in an ambient atmosphere, and n-channel transistors in a nitrogen glovebox.

The charge carrier mobility (μ) was calculated by fitting the saturation transfer characteristics using:

$$I_{DS} = \frac{WC}{2L}\mu(V_G - V_T)^2 \tag{2.14}$$

where I_{DS} is the drain current, W is the channel width, L is the channel length, C is the capacitance of the oxide, V_G is the gate voltage and V_T is the threshold voltage.

Appendix 2.A: Growth of a Kossel Crystal

Due to its significance on the mobility and conductivity of pentacene thin films, this appendix will introduce general concepts related to crystallization from the vapor phase, and the heterogeneous nucleation of 2D versus 3D crystals. A Kossel crystal is one where all the atoms/molecules are assumed to be cubic in geometry [18]. This is the simplest kind of crystal; more complex geometries often lead to equations which are analytically impossible to solve. Comparing with nucleation of a liquid droplet from a supersaturated vapor, the crystallization of solid crystals is more complex due to the various surfaces with their (often) distinct surface energies [18]. Consider a homogeneous (i.e., not on a substrate or surface) 3D Kossel crystal in equilibrium with the vapor phase (constant temperature and

constant volume) then the change in Helmholtz free energy (dF) is zero and can be expressed:

$$dF = -P_v dV_v - P_c dV_c + \sum_n \sigma_n dA_n = 0 \tag{2A.1}$$

$$-(P_c - P_v)dV_c + \sum_n \sigma_n dA_n = 0 \tag{2A.2}$$

where P_v is the pressure in the vapor phase, P_c is the vapor pressure of the crystal, V_v and V_c are the vapor and crystal volumes, σ_n is the surface energy of surface n with corresponding area A_n. Equation 2A.2 is the simplified form of Eq. 2A.1 since at equilibrium the total volume is constant (i.e. ($dV_v = -dV_c$)). The volume of a crystal can also be expressed as a sum of volumes of pyramids with heights h_n and areas A_n, as suggested by Wulff in 1901 [18, 38]. V_c and dV_c can then be expressed:

$$V_c = \frac{1}{3}\sum_n h_n A_n \tag{2A.3}$$

$$dV_c = \frac{1}{2}\sum_n A_n dh_n \tag{2A.4}$$

To second order, the very small changes to the total volume dV_c can be accounted for by assuming constant area with infinitesimal changes in pyramid height dh_n (see Markov, Ref. [18] for more details). Reinserting into Eq. 2A.2

$$\sum_n \left[\sigma_n - \frac{1}{2}(P_c - P_v)h_n\right] dA_n = 0 \tag{2A.5}$$

Since each of the changes in area (dA_n) are not related, the first term in the bracket must equal zero

$$P_c - P_v = 2\frac{\sigma_n}{h_n} = \text{constant} \tag{2A.6}$$

This is a restatement of Wulff's rule which states: "at equilibrium, the distances of the crystal faces from a point within a crystal (called Wulff's point which can arbitrarily be chosen as the center of the crystal) are proportional to their corresponding specific surface energies of these faces" [18, 38]. This concept is extremely important in determining whether 2D or 3D crystal growth dominates. Since the chemical potential difference is directly related to the difference in pressures of the two phases by the molar volume of the crystal phase (V_c), Eq. 2A.6 can also be written in a more convenient form:

$$\Delta u = u_v - u_v = 2\frac{\sigma_n v_c}{h_n} \tag{2A.7}$$

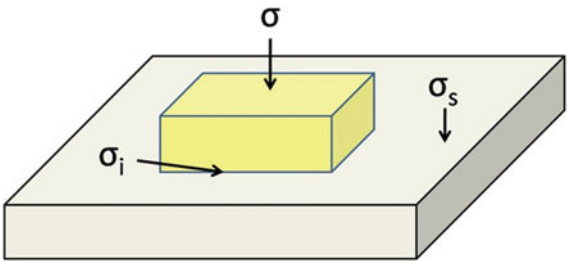

Fig. 2.9 The relevant surface/interfacial energies used to determine the equilibrium shape of a crystal

This is an important result which mathematically expresses the physical concept that that the supersaturation is the same over the crystal surface, and the growth mode (values of h_n) is directly related to the supersaturation. Again, the discussion above was given for a homogenous crystal. For heterogeneous nucleation, which is relevant for organic semiconductor nucleation in OTFTs, Eq. 2A.7 must be slightly modified to include the interaction or adhesion energy (σ_i) between the crystal and the substrate upon which it is nucleating:

$$\frac{\Delta u}{2v_c} = \frac{\sigma_0 - \sigma_1}{h_n} = \text{constant} \tag{2A.8}$$

where σ_o refers to the homogenous case (surface energy); when σ_i is zero then the homogenous Eq. 2A.7 is retained. For values where $h_n > 1$, 3D crystals will form, whereas for $h_n = 1$, desirable 2D nucleation prevails. Thus, the term $\sigma_{i,}$ which relates the strength of interaction between the semiconductor and the substrate is a key parameter in determining whether 2D or 3D growth will prevail [18]. The chemical potential driving force and the interfacial energies will determine the growth mode. Define the total change in surface energy upon nucleation on a foreign substrate by $\Delta\sigma$ where:

$$\Delta\sigma = \sigma + \sigma_i - \sigma \tag{2A.9}$$

σ is the surface energy of the crystal, σ_i is the interfacial surface energy (whose magnitude can be either positive or negative) and σ_s is the surface energy of the substrate [18]. There are three basic cases (Fig. 2.9).

Case 1: $\Delta\sigma < 0$, this case results when the interaction with the surface is greater than the interlayer interaction energies. Of course in this case, 3D nucleation is prohibited and 2D nucleation can occur at $\Delta\mu = 0$, and even at undersaturation $\Delta\mu < 0$ (provided that $|\Delta\mu| < |A_m\Delta\sigma|$ where A_m is molecular area).

Case 2: $\Delta\sigma = 0$ indicates a balanced force between interlayer interaction energy and molecule substrate interactions. This is the general case for nucleation for a material on it crystal of itself (homogenous nucleation). Again in this case, 3D nucleation is thermodynamically impossible, and 2D wetting occurs for supersaturated systems $\Delta\mu > 0$.

Case 3: $\Delta\sigma > 0$, or when the system's surface energy increases can give rise to both 2D and 3D growth depending on $\Delta\mu$. This is the general case which was

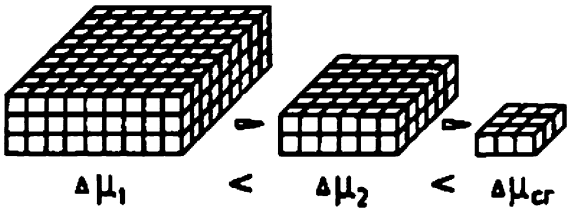

Fig. 2.10 A schematic showing how past the critical supersaturation a 3D Kossel crystal must become 2D in order to maintain equilibrium shape from Ref. [18]

discussed in Chap. 2. The barrier for 3D nucleation, ΔG^*_{3D}, is inversely related to $(\Delta\mu)^2$ (Eq. 2.3) and is possible for all values of $\Delta\mu > 0$. Again 2D nucleation becomes possible only at supersaturations greater than $\Delta\mu_2$, where the change in surface free energy upon nucleation is $\Delta\mu_2 = A_m\Delta\sigma$. This is a logical conclusion, since there must be a driving force greater than the gain in surface energy for nucleation, for the total free energy of the system to decrease. As $\Delta\mu$ increases beyond $\Delta\mu_2$, there exists a critical supersaturation $\Delta\mu_{cr}$ (where $\Delta\mu_{cr} = 2\Delta\mu_2$ at which the $\Delta G^*_{3D} = \Delta G^*_{2D}$) or consequently the height the 3D island is one monolayer high (i.e. a 2D crystal). The extension of Wulff's rule shows that under equilibrium a Kossel crystal will try to maintain its height/length ratio [18, 38] (Fig. 2.10).

In the analysis presented in this chapter on pentacene growth, the chemical potential driving force was fixed, and thus the energetics which determined growth mode are related to the interfacial energies. This allowed for estimation of the interaction energy between pentacene and the different OTS layers. In the following chapter it was determined that on crystalline OTS the pentacene molecule substrate interaction energy is greater than the interlayer interaction energy and in fact this would fall under *case 1* ($\Delta\sigma < 0$) presented above.

The important caveat which must be mentioned is that for systems far from equilibrium (high supersaturations) cannot be addressed using methodology discussed in this chapter, which use thermodynamic models for treating nucleation and crystal shape.

References

1. Bao Z, Locklin J (2007) Organic field effect transistors. CRC Press Taylor and Francis Group, Boca Raton
2. Dimitrakopoulos CD, Malenfant PRL (2002) Organic thin film transistors for large area electronics. Adv Mater 14:99-+
3. Dinelli F et al (2004) Spatially correlated charge transport in organic thin film transistors. Phys Rev Lett 92:116802
4. Kobayashi S et al (2004) Control of carrier density by self-assembled monolayers in organic field-effect transistors. Nat Mater 3:317–322
5. Heringdorf F, Reuter MC, Tromp RM (2001) Growth dynamics of pentacene thin films. Nature 412:517–520
6. Mayer AC, Ruiz R, Headrick RL, Kazimirov A, Malliaras GG (2004) Early stages of pentacene film growth on silicon oxide. Org Electron 5:257–263

7. Lin YY, Gundlach DJ, Nelson SF, Jackson TN (1997) Stacked pentacene layer organic thin-film transistors with improved characteristics. IEEE Electron Device Lett 18:606–608
8. Steudel S, Janssen D, Verlaak S, Genoe J, Heremans P (2004) Patterned growth of pentacene. Appl Phys Lett 85:5550–5552
9. Tang ML, Okamoto T, Bao ZN (2006) High-performance organic semiconductors: Asymmetric linear acenes containing sulphur. J Am Chem Soc 128:16002–16003
10. Tang ML, Reichardt AD, Miyaki N, Stoltenberg RM, Bao Z (2008) Ambipolar, high performance, acene-based organic thin film transistors. J Am Chem Soc 130:6064
11. Kelley TW et al (2004) Recent progress in organic electronics: materials, devices, and processes. Chem Mater 16:4413–4422
12. Veres J, Ogier S, Lloyd G, de Leeuw D (2004) Gate insulators in organic field-effect transistors. Chem Mater 16:4543–4555
13. Park YD, Lim JA, Lee HS, Cho K (2007) Interface engineering in organic transistors. Mater Today 10:46–54
14. Yang SY, Shin K, Park CE (2005) The effect of gate-dielectric surface energy on pentacene morphology and organic field-effect transistor characteristics. Adv Funct Mater 15:1806–1814
15. Gundlach DJ, Kuo CC, Nelson SF, Jackson TN (1999) Organic thin film transistors with field effect mobility > 2 cm/sup 2//V-s. In: 1999 57th annual device research conference digest (Cat. No.99TH8393). doi:10.1109/DRC.1999.806357
16. Aizenberg J, Black AJ, Whitesides GM (1999) Control of crystal nucleation by patterned self-assembled monolayers. Nature 398:495–498
17. Lee HS et al (2008) Effect of the phase states of self-assembled monolayers on pentacene growth and thin-film transistor characteristics. J Am Chem Soc 130:10556–10564
18. Markov I (2003) Crystal growth for beginners: fundamentals of nucleation, crystal growth and epitaxy, 2nd edn. World Scientific, New Jersey
19. Verlaak S, Steudel S, Heremans P, Janssen D, Deleuze MS (2003) Nucleation of organic semiconductors on inert substrates. Phy Rev B 68:195409
20. Klauk H et al (2002) High-mobility polymer gate dielectric pentacene thin film transistors. J Appl Phys 92:5259–5263
21. Liu SH, Wang WCM, Briseno AL, Mannsfeld SCE, Bao ZN (2009) Controlled deposition of crystalline organic semiconductors for field-effect-transistor applications. Adv Mater 21:1217–1232
22. Lukas S, Sohnchen S, Witte G, Woll C (2004) Epitaxial growth of pentacene films on metal surfaces. Chemphyschem 5:266–270
23. Mannsfeld SCB, Virkar A, Reese C, Toney MF, Bao ZN (2009) Precise structure of pentacene monolayers on amorphous silicon oxide and relation to charge transport. Adv Mater 21:2294
24. Zhang XH, Domercq B, Kippelen B (2007) High-performance and electrically stable C-60 organic field-effect transistors. Appl Phys Lett 91:92114
25. Ulman A (1991) An introduction to ultrathin organic films from Langmuir–Blodgett to self assembly. Academic Press, San Diego
26. Francis R, Louche G, Duran RS (2006) Effect of close packing of octadecyltriethoxysilane molecules on monolayer morphology at the air/water interface. Thin Solid Films 513:347–355
27. Locklin J, Ling MM, Sung A, Roberts ME, Bao ZN (2006) High-performance organic semiconductors based on fluorene-phenylene oligomers with high ionization potentials. Adv Mater 18:2989
28. Porter MD, Bright TB, Allara DL, Chidsey CED (1987) Spontaneously organized molecular assemblies.4. structural characterization of normal-alkyl thiol monolayers on gold by optical ellipsometry, infrared-spectroscopy, and electrochemistry. J Am Chem Soc 109:3559–3568
29. Lee SH, Saito N, Takai O (2007) The importance of precursor molecules symmetry in the formation of self-assembled monolayers. Jpn J Appl Phys Part 1 Regul Pap Br Commun Rev Pap 46:1118–1123

30. Steudel S et al (2004) Influence of the dielectric roughness on the performance of pentacene transistors. Appl Phys Lett 85:4400–4402
31. Chabinyc ML et al (2004) Short channel effects in regioregular poly(thiophene) thin film transistors. J Appl Phys 96:2063–2070
32. Necliudov PV, Shur MS, Gundlach DJ, Jackson TN (2003) Contact resistance extraction in pentacene thin film transistors. Solid-State Electron 47:259–262
33. Dodabalapur A, Torsi L, Katz HE (1995) Organic transistors—2-dimensional transport and improved electrical characteristic. Science 268:270–271
34. Ruiz R et al (2004) Structure of pentacene thin films. Appl Phys Lett 85:4926–4928
35. Yang HC et al (2005) Conducting AFM and 2D GIXD studies on pentacene thin films. J Am Chem Soc 127:11542–11543
36. Ohring M (2001) The material science of thin films, 2nd edn. Academic Press, Orlando
37. Wakayama N, Inokuchi H (1967) Heats of sublimation of polycyclic aromatic hydrocarbons and their molecular packings. Bull Chem Soc Jpn 40:2267
38. Wulff G (1901) On the question of speed of growth and dissolution of crystal surfaces. Zeitschrift Fur Krystallographie Und Mineralogie 34:449–530

Springer

http://www.springer.com/978-1-4419-9703-6

Investigating the Nucleation, Growth, and Energy Levels of Organic Semiconductors for High Performance Plastic Electronics

Virkar, A.

2012, XII, 132 p., Hardcover
ISBN: 978-1-4419-9703-6